Supplement to: Hauck et al: Seasonally different carbon flux changes in the Southern Ocean in response to the Southern Annular Mode

1 Model

1.1 Initialisation

The model is initialised with the January salinity, temperature and nitrate fields of the World Ocean Atlas 2009 (WOA09) (*Locarnini et al.*, 2010; *Antonov et al.*, 2010; *Garcia et al.*, 2010) and with mean ALK and preindustrial DIC fields (GLODAP, *Key et al.*, 2004). The initial field for dissolved iron is obtained from PISCES output (*Aumont et al.*, 2003) after applying a correction based on observed profiles (*de Baar et al.*, 1999; *Boye et al.*, 2001) to reduce a high iron bias in the Southern Ocean. Sea surface salinity (SSS) and the full water column alkalinity field are restored to the Common Ocean-Ice Reference Experiment (CORE) surface salinity field (*Large and Yeager*, 2004) and the initial alkalinity field, with a time scale of one year.

The model is spun up from 1900 to 1947 with climatological (repeat mean year) forcing fields of the CORE data set (*Large and Yeager*, 2004). We use 6-hourly 10 m winds, 2 m air temperature, humidity and sea level pressure, daily downward long and short wave radiation fields and monthly precipitation. We apply a constant runoff field that is corrected for the missing freshwater fluxes from the Arctic ($0.08-0.17$ Sv *Dai and Trenberth*, 2002) by adding 0.08 Sv of runoff along the northern boundary of the domain which improves the overturning circulation. Wind stress, heat and freshwater fluxes are calculated from the forcing fields with bulk formulae (*Large and Yeager*, 2004). The freshwater and salinity balances are maintained globally by a normalisation procedure (*Griffies et al.*, 2009).

After the spin-up, the period from 1948 to 2010 is simulated using 6-hourly forcing fields from the NCEP/NCAR-R1 data product where available and daily fields otherwise (*Kalnay et al.*, 1996, updated 2011). The runoff field remains the same as in the spin-up. We use monthly dust data for 1979 to 2010, based on *Mahowald et al.* (2003), with slight modifications to the dust transport parameterizations, to sustain a closer agreement to

observations (N. Mahowald, pers. comm.). Dust is deposited on a monthly basis from 1979 onwards. Up to the year 1978 a monthly climatological dust deposition field is used, calculated from the 1979-2010 data.

1.2 Simulations

We perform two baseline runs to differentiate between natural and anthropogenic carbon fluxes; a control run (CTRL) with constant atmospheric CO_2 of 278 ppm and a run with inter-annually varying CO_2 (VAR) according to the reconstructed atmospheric CO_2 concentrations (*Enting et al.*, 1994) until 1958 and to the Mauna Loa observatory data from 1959 onwards (ftp://ftp.cmdl.noaa.gov/ccg/co2/trends/co2_mm_mlo.txt). Only the CTRL run is used for the analysis in the main manuscript.

The term "natural" CO_2 flux refers to the model run with preindustrial atmospheric CO_2 forcing (CTRL) in contrast to "anthropogenic" CO_2, which is defined as the difference between the model runs with preindustrial (CTRL) and contemporary (VAR) CO_2 forcing. Yet, the "natural" CO_2 flux is also affected by anthropogenic activities, as the wind forcing has changed since preindustrial times due to the ozone hole and greenhouse gas emissions. All results for the mean model state in this supplement are shown for the contemporary model run (VAR), if not stated otherwise, to be comparable to the available data sets, whereas the analysis on the inter-annual variability of carbon fluxes in the main manuscript is conducted with results from the CTRL run to analyse the effects of perturbed atmospheric forcing.

We investigate the inter-annual variability (IAV) in the fluxes of natural carbon in the Southern Ocean. While the VAR simulation is useful for model validation, we find that most of the IAV in the contemporary Southern Ocean CO_2 fluxes ($1\sigma = 0.23$ Pg C yr^{-1}) is driven by IAV in the natural fluxes (0.21 Pg C yr^{-1}), i.e. anthropogenic fluxes exhibit only small IAV (0.07 Pg C yr^{-1}). These results are consistent with those presented in Lov07.

2 Mean model state

2.1 Southern Ocean circulation and nutrient fields

In the period with inter-annually varying forcing, the monthly, vertically integrated zonal flow through Drake Passage fluctuates between 117 and 138 Sv which is within the range of the transport estimated from observations (*Cunningham et al.*, 2003; *Orsi et al.*, 1995; *Whitworth*, 1983; *Whitworth and Peterson*, 1985). In our simulation, the ACC transport shows a weak positive trend between 1955 and 1975, followed by a period of relative stability (Figure 1a). Thus, the Drake Passage transport in our model appears to be sufficiently stable and realistic over the study period (1948-2010). The barotropic stream function (Figure 1b) with the typical southeastward route from the western Atlantic to the Eastern Pacific and the northward expansion east of the Drake Passage also agrees with other simulations (e.g., *Griffies et al.*, 2009).

The model agreement with WOA09 and GLODAP data is within an expected range for both annual mean and seasonal 3D fields of potential temperature, salinity, nitrate

and silicate (south of 30°S, Figure 2a). When the total water column is considered, all correlation coefficients are better than 0.86 for both annual average and mean seasonal cycle. The standard deviation in the modelled salinity, alkalinity and silicate fields differs from that in the data fields by a factor between 0.99 and 1.02. The standard deviations of potential temperature, nitrate and DIC are between 7% and 12% higher than in the observations, indicating that gradients are slightly overestimated.

In the surface layer, differences between annual average and seasonal fields become more pronounced (Figure 2b). Potential temperature is very well reproduced due to the atmospheric forcing. Annual and seasonal silicate distributions have correlation coefficients of 0.87 and 0.65, respectively, and normalised standard deviations <1, i.e. gradients are underestimated. Salinity, alkalinity and DIC have correlation coefficients >0.9 and normalised standard deviations of 1 to 1.2. The seasonal signals of silicate and nitrate have lower normalised standard deviations than the annual average, indicating that the seasonal cycle is too weak in the model. The opposite can be observed for salinity, where the standard deviation of the annual average is 3% higher than in the data, but the variability of the seasonal cycle is overestimated by 22%.

As the model was initialised with WOA09 and GLODAP fields, this demonstrates that the model represents the processes that determine nutrient distribution (i.e., biological production and remineralisation) reasonably well, that the model drift is small over the short period considered, and that appropriate boundary conditions for heat and freshwater fluxes are applied.
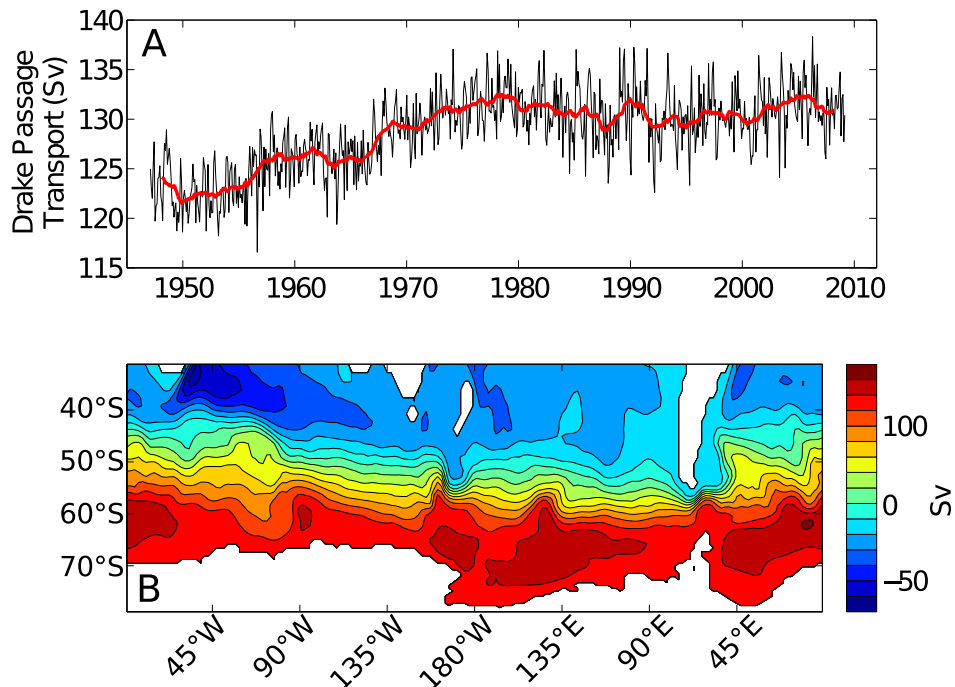

Figure 1: Modeled Southern Ocean circulation. (a) Time-series of Drake Passage transport (Sv), black: monthly average, red: running mean over two years, (b) Mean barotropic streamfunction (Sv) between 1948 and 2010.
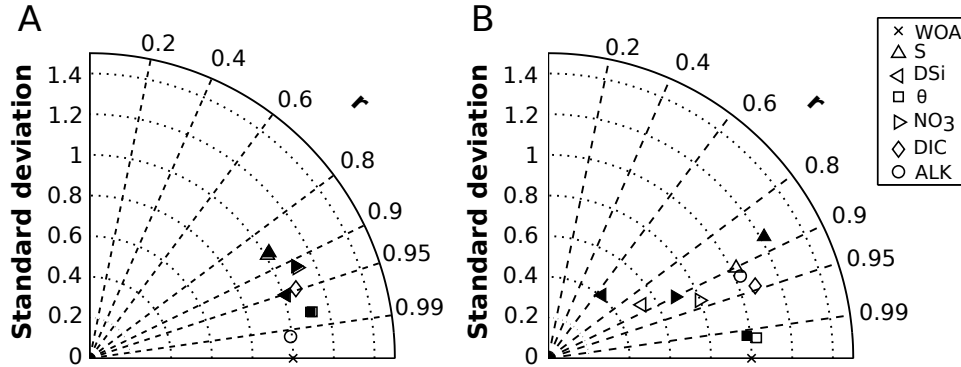
Figure 2: Taylor diagrams (normalised standard deviation and correlation coefficient r) comparing model salinity, temperature, nitrate and silicate fields to World Ocean Atlas 09 data, and DIC and alkalinity fields to GLODAP. Annual average (open symbols) and mean seasonal cycle (filled symbols) were calculated for the domain south of 30°S and the period 1948 to 2010. The standard deviation is normalised to the standard deviation of the reference data. (a) 3D fields of the entire water column <30°S weighted by volume, (b) 2D surface field <30°S weighted by area.

2.2 Phytoplankton growth limitation and distribution

We determine the factors limiting phytoplankton nutrient uptake from the Michaelis-Menten factors (f_i) relating concentration of nutrient i (N_i) to the sum of N_i and the corresponding half saturation constant (K_i): $f_i = N_i/(K_i + N_i)$. The smallest Michaelis-Menten factor f_i indicates the most limiting nutrient. In the case that all nutrients (nitrate, silicate, iron) yield a Michaelis-Menten factor above 0.7, light, temperature or grazing or a combination of those are supposed to control phytoplankton growth or accumulation (*Schneider et al.*, 2008). Small phytoplankton growth in the Southern Ocean is largely limited by iron, macro nutrient limitation only appears sporadically north of 40°S (Figure 3). In vast areas, small phytoplankton is not limited by nutrients between May and October; light likely plays an important role during winter. In November, iron limitation becomes dominant as irradiance increases and persists throughout the summer. Diatoms are mostly limited by iron south of 50 to 60°S and by silicate to the north of that. The shift from iron to silicate limitation for diatom growth occurs approximately north of 60°S in the Pacific sector. It takes place further north, between 50 and 60°S in the Indian and Atlantic sectors. Light limitation appears in few areas between June and December. As the summer season proceeds, iron limitation spreads also north of the Polar Front, particularly in the Pacific. In the Southern Ocean, which is a high nutrient-low chlorophyll (HNLC) region (*de Baar et al.*, 1990; *Boyd et al.*, 2000), our model reproduces the crucial role of iron limitation, however, the iron limited areas spread too far north. Our simulations indicate silicate limitation for diatoms north of the PF in agreement with observations (*Jacques*, 1983; *Boyd et al.*, 1999).

Diatoms dominate phytoplankton biomass and chlorophyll south of 50°S (Figure 4). Their contribution to standing stocks in terms of carbon and chlorophyll is reduced to less than 20% north of that limit in agreement with observations (*de Baar et al.*, 1999).

The Indian sector and the continental margins are exceptions to that rule; here, diatoms can be responsible for up to 50% of the biomass north of 50°S (Figure 4b). These exceptional maxima were attributed to intensified iron deposition from dust (*Aumont et al.*,
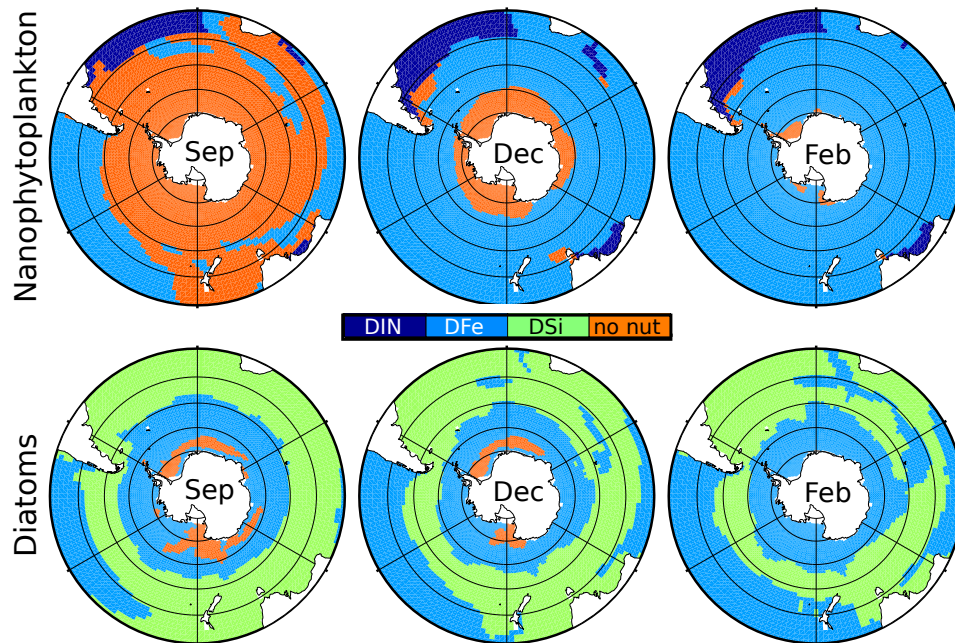

Figure 3: Most limiting factors for (top row) nanophytoplankton and (bottom row) diatom growth in (from left to right) spring (September), summer (December) and autumn (February): nitrate (dark blue), iron (light blue), silicate (green), light/temperature/grazing (orange). When no nutrient is limiting with a Michaelis Menten coefficient below 0.7, we assume that light, temperature (and grazing for nanophytoplankton) are limiting (*Schneider et al.*, 2008). See text for further explanation.
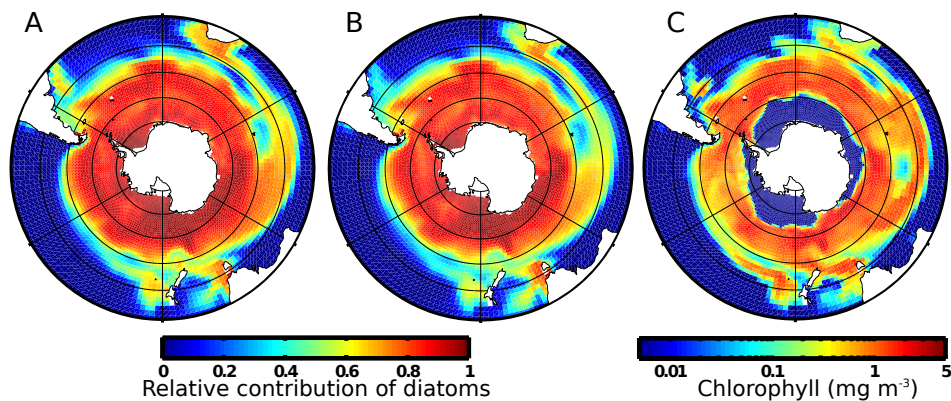

Figure 4: Relative contribution (mean of model years 1948 to 2010) of diatoms to surface (a) chlorophyll and (b) phytoplankton carbon (0 = 0%, 1 = 100%). (c) Surface diatom chlorophyll averaged over October and November 2005 to be comparable to *Bracher et al.* (2009).
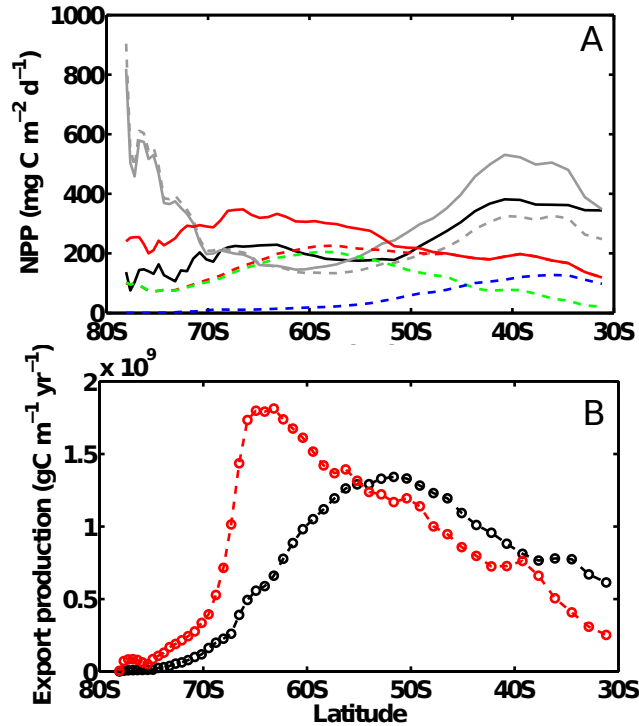
Figure 5: Primary and export production, (a) Vertically integrated net primary production in mg C m^{-2} d^{-1}. VGPM (gray line) and Eppley (gray dashed line) are chlorophyll-based satellite-derived estimates (*Behrenfeld and Falkowski*, 1997), CBPM (black line) is a chlorophyll and carbon-based satellite-derived estimate and is considered a significant improvement to VGPM and Eppley (*Westberry et al.*, 2008). The model output (red dashed line) is biased (red line) to cover the same time as the satellite-based estimates. Also shown are the contributions of diatoms (green dashed line) and nanophytoplankton (blue dashed line). (b) Zonally integrated export production at 100 m reported per m in meridional direction (g C m^{-1} yr^{-1}), black symbols: estimate from *Schlitzer* (2002), red symbols: model output. Note that the latitudinal spacing is not equidistant, so that locally higher modelled zonal integrals in the south level out with lower zonal integrals in the north when integrated over the entire area.

2003). Diatom chlorophyll (Figure 4c) shows the same gradient from low chlorophyll north of about 45 to 50°S to high chlorophyll between 50°S and 60°S as in satellite-derived estimates (*Bracher et al.*, 2009).

The zonal averaged vertically integrated net primary production (NPP, Figure 5) follows the same pattern as satellite-based estimates (*Behrenfeld and Falkowski*, 1997; *Westberry et al.*, 2008). In the Southern Ocean, there are two peaks. The first peak is around 40°S, and is dominated by nanophytoplankton in the model. The second peak occurs in the model and in the 'chlorophyll and carbon-based' satellite estimate (CBPM, *Westberry et al.* (2008)) at about 60°S and is dominated by diatoms. It is followed by a decrease further to the south. In the two 'chlorophyll-based' satellite derived estimates (VGPM and Eppley, *Behrenfeld and Falkowski* (1997)), there is just one peak in NPP between about

60°S and the southern end of the domain. The CBPM algorithm to derive net primary production is considered a significant improvement compared to VGPM and Eppley, as it consciously takes into account the decoupling of carbon and chlorophyll and is validated against field data (*Westberry et al.*, 2008). Thus, we argue that the increase towards 80°S represents an overestimation by the VGPM and Eppley products. The model estimate of the diatom belt around 60°S, however, is somewhat higher than in all satellite-based estimates. This might be an artifact of known underestimation of SeaWiFS chlorophyll by 50% in the Southern Ocean (*Szeto et al.*, 2011), but might also indicate a model bias. The integrated model POC export at 100 m south of 30°S is 4.6 Pg C yr^{-1}, which is 15% more than the estimate of *Schlitzer* (2002) that amounts to 4 Pg C yr^{-1}. The additional export is produced between 60 and 70°S where the modelled export production is higher than the Schlitzer estimate. This peak, however, is in line with the peak in modelled and observed NPP (CBPM) and it remains unclear which estimate is more trustworthy.

2.3 Carbonate system

2.3.1 Contemporary carbonate system

The surface distributions of DIC and ALK determine the partial pressure of CO_2 in seawater and by that the CO_2 exchange with the atmosphere. DIC is controlled by advection
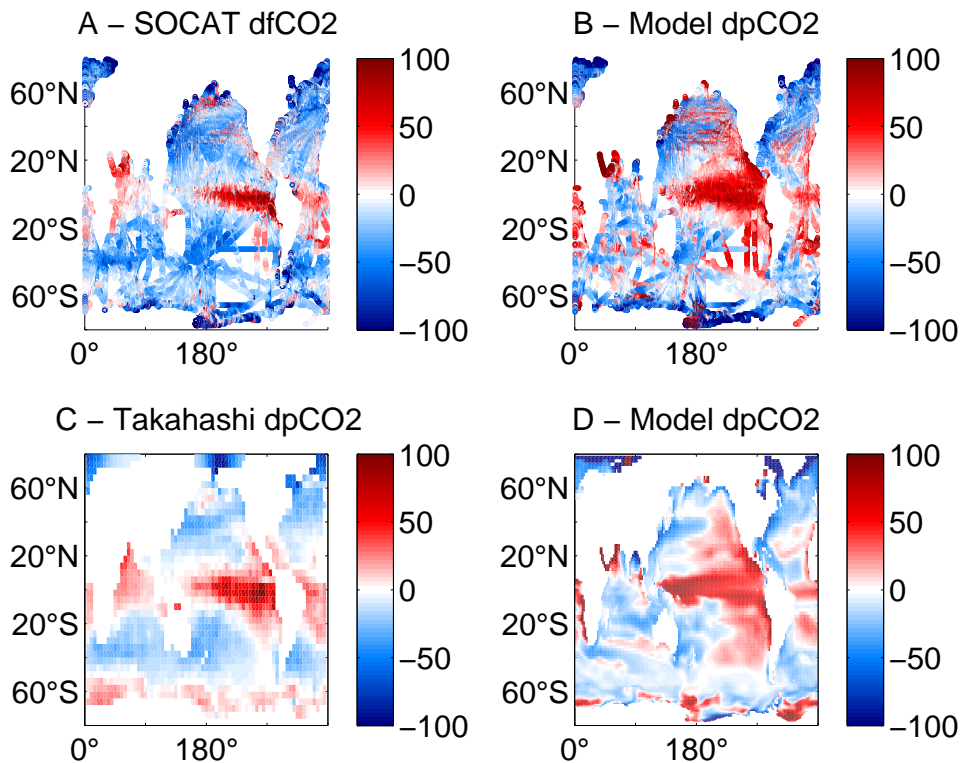

Figure 6: Model-data comparison of ΔpCO_2 (μatm), (a) SOCAT data, non-gridded, (b) model results at time and location where SOCAT data is available, (c) Takahashi ΔpCO_2, gridded, annual mean 2000, (d) model results, annual mean for 2000.

and diffusion, by sea-air gas exchange, drawdown by primary production, release during respiration and remineralization and by $CaCO_3$ production and dissolution. The reproduction of spatial patterns of DIC and (restored) alkalinity compares well with GLODAP (correlation coefficients > 0.9, normalised standard deviation close to one) for the full water column and the surface as seen in the Taylor plots (Figure 2).

We compare surface ΔpCO_2 to both the ungridded SOCAT (*Pfeil et al.*, 2012) and the interpolated Takahashi (*Takahashi et al.*, 2009) database. For the comparison with SOCAT, only model output from the same month and at the same location are plotted, whereas the complete surface field averaged over the year 2000 is plotted versus the Takahashi data set (Figure 6). Both comparisons show that the general patterns are well captured, however, the regions where the model predicts oversaturation are too widespread. Along the Antarctic continent, the model shows both strong undersaturation at the SOCAT sampling points, and oversaturation in the annual mean as in the Takahashi data base.
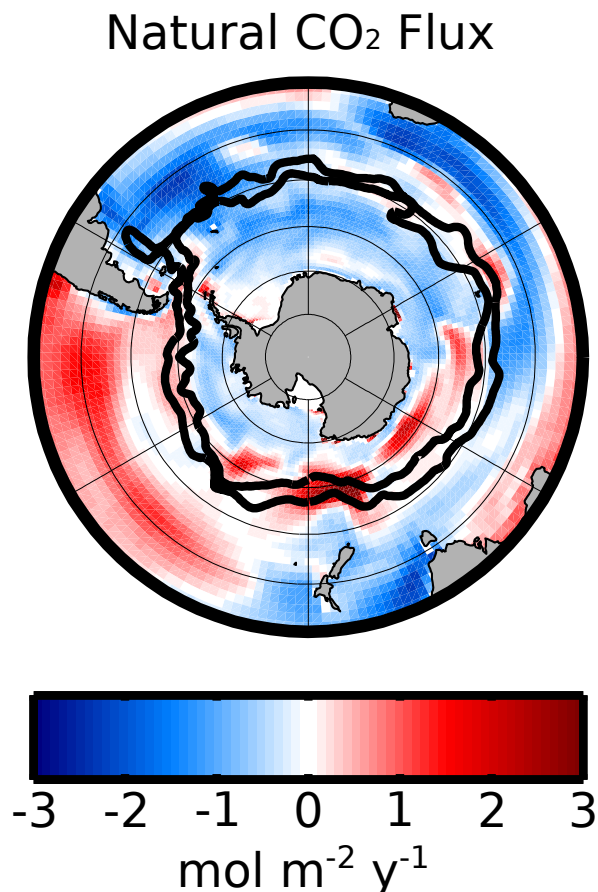

Figure 7: Modelled natural CO_2 flux (mean 1948-2010, negative means into the ocean)

2.3.2 Natural CO$_2$ fluxes

Figure 7 shows the average CO$_2$ flux between 1948 and 2010 from the CTRL run, i.e. the natural CO$_2$ flux. In line with previous studies there are regions where uptake of CO$_2$ occurs and others where CO$_2$ is released (*Lovenduski et al.*, 2007; *Dufour*, 2011; *Mikaloff Fletcher et al.*, 2007). The generally assumed preindustrial outgassing signal in the polar Southern Ocean south of 58°S (*Mikaloff Fletcher et al.*, 2007) is too weak in our model. This might be due to the fact that after about 100 years of model simulation the three-dimensional distributions of carbon, alkalinity and nutrients have not reached a quasi-steady state, and consequently the air-sea carbon flux is not yet equilibrated. The assumption made implicitly here (and in a large set of other studies) is that the system is sufficiently close to linear that a bias in the mean state does not affect our analysis of SAM-driven changes in carbon fluxes.
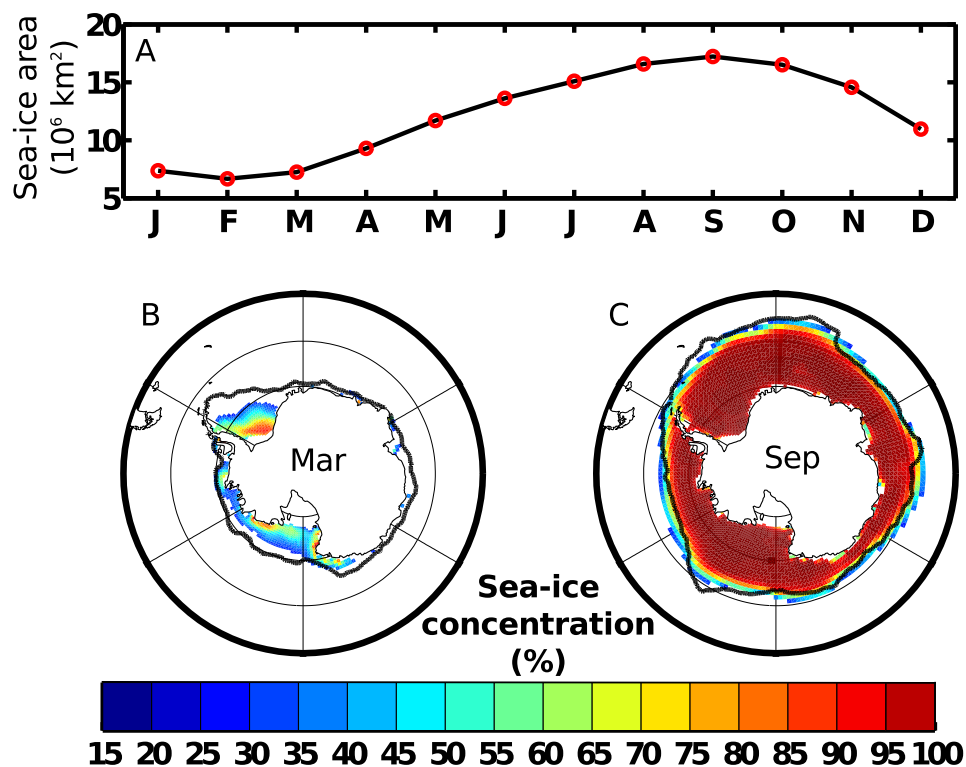

Figure 8: Modelled sea-ice extent. (a) Mean seasonal cycle of sea-ice area between 1979 and 2010. Sea-ice concentration (%) in (b) March and in (c) September, at the maximum of sea-ice area. Modeled sea-ice area is shown above 15%, the black solid line marks the corresponding 15% isoline from satellite data for comparison.

3 Seasonal cycle

3.1 Sea ice

We reproduce a reasonable seasonal sea-ice distribution in the Southern Hemisphere (Figure 8). The minimum sea-ice extent (averaged over the period 1979 to 2010 to be comparable with observations) occurs in February; the maximum is found in September. Timing and magnitude are in line with passive microwave satellite data (*Cavalieri and Parkinson*, 2008), although the sea-ice extent at its minimum is lower than in observations. Other studies suggest that the realism of the simulated sea-ice fields depends on the resolution of the model grid (e.g., *Losch et al.*, 2010). In our simulation, the annual mean of the total sea-ice area varies between 1.2 and 1.3 x 10^{13} m^2 which compares well to the estimate of about 10^{13} m^2 (*Comiso*, 1999; *Griffies et al.*, 2009) and is similar to the performance of other coarse grid ocean-ice models (*Griffies et al.*, 2009).

3.2 Chlorophyll

We compare the seasonal cycle of chlorophyll south of 30°S in the period 2003-2010 (VAR run) with a satellite-derived chlorophyll seasonal cycle (GLOBCOLOUR, 2003-2010, calculated from monthly binned data) in Figure 9. The modelled estimate for total chlorophyll is within the range of satellite estimates between December and September. It captures the amount of chlorophyll in summer and the decrease in autumn and winter reasonably well. It overestimates the amount of chlorophyll in October and November and the maximum chlorophyll concentration occurs one month too early in the model as compared to the satellite data (November instead of December).

By and large, we present a model set-up that simulates Southern Ocean circulation
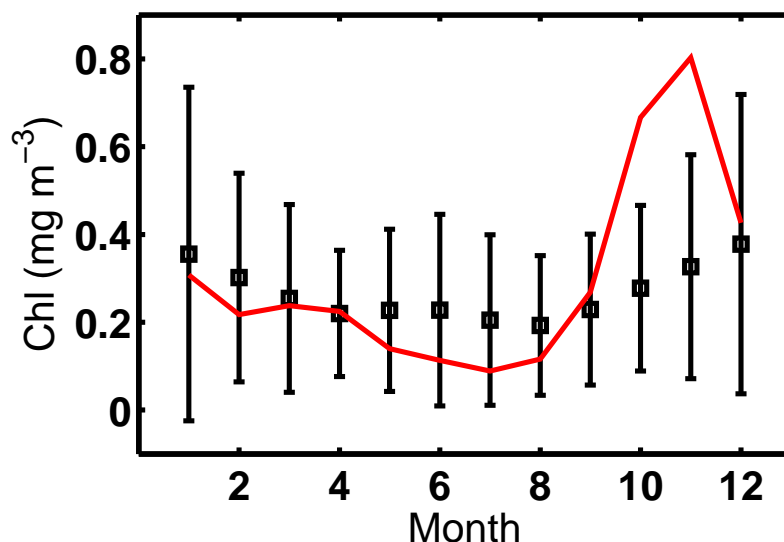

Figure 9: Seasonal cycle of surface chlorophyll (mg m^{-3}). Red: mean model seasonal cycle 2003 - 2010. Black: mean seasonal cycle of satellite-derived chlorophyll data 2003 - 2010, square: monthly mean, error bar: one standard deviation.
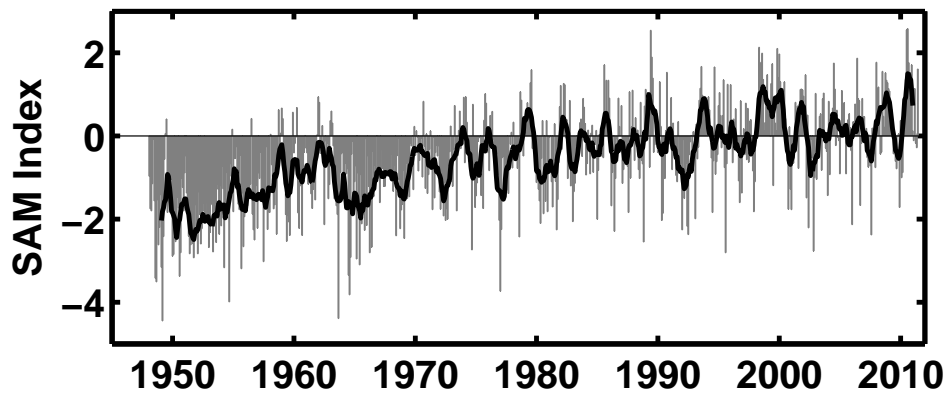
Figure 10: SAM Index, grey bars: SAM Index as downloaded from http://jisao.washington.edu/data/aao/slp; black line: smoothed SAM Index, smoothed by applying an 8-months running mean filter.

processes, thermodynamics and core biological processes with satisfactory realism. It is appropriate for the study of carbon fluxes that are controlled by a complex interplay of thermal effects, wind forcing, circulation patterns and biological interaction.

4 SAM

Figure 10 shows the raw SAM index from 1948 to 2010 based on the leading EOF of sea-level pressure anomalies south of 20°S from the NCEP-NCAR Reanalysis. The SAM index is standardised to the period 1979 to 2010 with a mean of zero and a standard deviation of one. In addition, Figure 10 shows the smoothed SAM index where a running eight months mean filter was applied.

References

Antonov, J. I., D. Seidov, T. P. Boyer, R. A. Locarnini, A. V. Mishonov, H. E. Garcia, O. K. Baranova, M. M. Zweng, and D. R. Johnson (2010), World Ocean Atlas 2009, Volume 2: Salinity, in *NOAA Atlas NESDIS 69*, edited by S. Levitus, p. 184, U.S. Government Printing Office, Washington, D.C.

Aumont, O., E. Maier-Reimer, S. Blain, and P. Monfray (2003), An ecosystem model of the global ocean including Fe, Si, P colimitations, *Global Biogeochemical Cycles*, *17*, 1060, doi:10.1029/2001GB001745.

Behrenfeld, M. J., and P. G. Falkowski (1997), Photosynthetic rates derived from satellite-based chlorophyll concentration, *Limnology and Oceanography*, *42*, 1–20, doi:10.4319/lo.1997.42.1.0001.

Boyd, P., J. LaRoche, M. Gall, R. Frew, and R. M. L. McKay (1999), Role of iron, light, and silicate in controlling algal biomass in subantarctic waters SE of New Zealand, *Journal of Geophysical Research*, *104*, 13,395–13,408, doi:10.1029/1999JC900009.

Boyd, P. W., A. J. Watson, C. S. Law, E. R. Abraham, T. Trull, R. Murdoch, D. C. E. Bakker, A. R. Bowie, K. O. Buesseler, H. Chang, M. Charette, P. Croot, K. Downing, R. Frew, M. Gall, M. Hadfield, J. Hall, M. Harvey, G. Jameson, J. LaRoche, M. Liddicoat, R. Ling, M. T. Maldonado, R. M. McKay, S. Nodder, S. Pickmere, R. Pridmore, S. Rintoul, K. Safi, P. Sutton, R. Strzepek, K. Tanneberger, S. Turner, A. Waite, and J. Zeldis (2000), A mesoscale phytoplankton bloom in the polar Southern Ocean stimulated by iron fertilization, *Nature*, *407*, 695–702, doi:10.1038/35037500.

Boye, M., C. M. G. van den Berg, J. T. M. de Jong, H. Leach, P. Croot, and H. J. W. de Baar (2001), Organic complexation of iron in the Southern Ocean, *Deep-Sea Research I*, *48*, 1477–1497, doi:10.1016/S0967-0637(00)00099-6.

Bracher, A., M. Vountas, T. Dinter, J. P. Burrows, R. Röttgers, and I. Peeken (2009), Quantitative observation of cyanobacteria and diatoms from space using PhytoDOAS on SCIAMACHY data, *Biogeosciences*, *6*, 751–764, doi:10.5194/bg-6-751-2009.

Cavalieri, D. J., and C. L. Parkinson (2008), Antarctic sea ice variability and trends, 1979-2006, *Journal of Geophysical Research*, *113, C07004*, doi:10.1029/2007JC004564.

Comiso, J. (1999), Bootstrap sea ice concentrations for NIMBUS-7 SMMR and DMSP SSM/I, June to September 2001. National Snow and Ice Data Center Digital Media, *19*.

Cunningham, S. A., S. G. Alderson, B. A. King, and M. A. Brandon (2003), Transport and variability of the Antarctic Circumpolar Current in Drake Passage, *Journal of Geophysical Research*, *108*, 8084, doi:10.1029/2001JC001147.

Dai, A., and K. E. Trenberth (2002), Estimates of freshwater discharge from continents: Latitudinal and seasonal variations, *Journal of Hyrdmeteorology*, *3*, 660–687.

de Baar, H. J. W., A. G. J. Buma, R. F. Nolting, G. C. Cadée, G. Jacques, and P. J. Tréguer (1990), On iron limitation of the Southern Ocean: experimental observations in the Weddell and Scotia Seas, *Marine Ecology-Progress Series*, *65*, 105–122, doi: 10.3354/meps065105.

de Baar, H. J. W., J. T. M. de Jong, R. F. Nolting, K. R. Timmermans, M. A. van Leeuwe, U. Bathmann, M. Rutgers van der Loeff, and J. Sildam (1999), Low dissolved Fe and the absence of diatom blooms in remote Pacific waters of the Southern Ocean, *Marine Chemistry*, *66*, 1–34, doi:10.1016/S0304-4203(99)00022-5.

Dufour, C. (2011), Rôle des tourbillons océaniques dans la variabilité récente des flux air-mer de CO_2 dans l'océan Austral, *PhD Thesis, Université de Grenoble*.

Enting, I. E., T. M. L. Wigley, and M. Heimann (1994), Future emissions and concentrations of carbon dioxide: Key ocean/atmosphere/land analyses, *CSIRO Division of Atmospheric Research Technical Paper*, *31*.

Garcia, H. E., R. A. Locarnini, T. P. Boyer, J. I. Antonov, M. M. Zweng, O. K. Baranova, and D. R. Johnson (2010), World Ocean Atlas 2009, Volume 4: Nutrients (phosphate, nitrate, and silicate), in *NOAA Atlas NESDIS 71*, edited by S. Levitus, p. 398, U.S. Government Printing Office, Washington, D.C.

Griffies, S., A. Biastoch, C. Böning, F. Bryan, G. Danabasoglu, E. Chassignet, M. England, R. Gerdes, H. Haak, R. Hallberg, W. Hazeleger, J. Jungclaus, W. G. Lagre, G. Madec, A. Pirani, B. L. Samuels, M. Scheinert, A. Sen Gupta, C. A. Severijns, H. L. Simmons, A. M. Treguier, M. Winton, S. Yeager, and J. Yin (2009), Coordinated Ocean-Ice Reference Experiments (COREs), *Ocean Modelling*, *26*, 1–46, doi: 10.1016/j.ocemod.2008.08.007.

Jacques, G. (1983), Some ecophysiological aspects of the Antarctic phytoplankton, *Polar Biology*, *2*, 27–33, doi:10.1007/BF00258282.

Kalnay, E., M. Kanamitsu, R. Kistler, W. Collins, D. Deaven, L. Gandin, M. Iredell, S. Saha, G. White, J. Woollen, Y. Zhu, M. Chelliah, W. Ebisuzaki, W. Higgins, J. Janowiak, K. C. Mo, C. Ropelewski, J. Wang, A. Leetmaa, R. Reynolds, R. Jenne, and D. Joseph (1996), The NCEP/NCAR 40-year reanalysis project, *Bulletin of the American Meteorological Society*, *77*, 437–471.

Key, R. M., A. Kozyr, C. L. Sabine, K. Lee, R. Wanninkhof, J. L. Bullister, R. A. Feely, F. J. Millero, C. Mordy, and T.-H. Peng (2004), A global ocean carbon climatology: Results from Global Data Analysis Project (GLODAP), *Global Biogeochemical Cycles*, *18, GB4031*, doi:10.1029/2004GB002247.

Large, W. G., and S. G. Yeager (2004), Diurnal to decadal global forcing for ocean and sea-ice models: The data sets and flux climatologies, *NCAR Technical Note*.

Locarnini, R. A., A. V. Mishonov, J. I. Antonov, T. P. Boyer, H. E. Garcia, O. K. Baranova, M. M. Zweng, and D. R. Johnson (2010), World Ocean Atlas 2009, Volume 1: Temperature, in *NOAA Atlas NESDIS 68*, edited by S. Levitus, p. 184, U.S. Government Printing Office, Washington, D.C.

Losch, M., D. Menemenlis, J.-M. Campin, P. Heimbach, and C. Hill (2010), On the formulation of sea-ice models. Part 1: Effects of different solver implementations and parameterizations, *Ocean Modelling*, *33*, 129–144, doi:10.1016/j.ocemod.2009.12.008.

Lovenduski, N. S., N. Gruber, S. C. Doney, and I. D. Lima (2007), Enhanced CO_2 outgassing in the Southern Ocean from a positive phase of the Southern Annular Mode, *Global Biogeochemical Cycles*, *21, GB2026*, doi:10.1029/2006GB002900.

Mahowald, N., C. Luo, J. del Corral, Zender, and S. C (2003), Interannual variability in atmospheric mineral aerosols from a 22-year model simulation and observational data, *Journal of Geophysical Research*, *108*, 4352, doi:10.1029/2002JD002821.

Mikaloff Fletcher, S. E., N. Gruber, A. R. Jacobson, M. Gloor, S. C. Doney, S. Dutkiewicz, M. Gerber, M. Follows, F. Joos, K. Lindsay, D. Menemenlis, A. Mouchet, S. A. Müller, and J. L. Sarmiento (2007), Inverse estimates of the oceanic sources and sinks of natural CO_2 and the implied oceanic carbon transport, *Global Biogeochemical Cycles*, *21, GB1010*, doi:10.1029/2006GB002751.

Orsi, A. H., T. Whitworth, and Others (1995), On the meridional extent and fronts of the Antarctic Circumpolar Current, *Deep Sea Research Part I: Oceanographic Research Papers*, *42*, 641–673, doi:10.1016/0967-0637(95)00021-W.

Pfeil, B., A. Olsen, D. C. E. Bakker, and et al. (2012), A uniform, quality controlled Surface Ocean CO_2 Atlas (SOCAT), *Earth System Science Data Discussions*, *5*, 735–780, doi:10.5194/essdd-5-735-2012.

Schlitzer, R. (2002), Carbon export fluxes in the Southern Ocean: results from inverse modeling and comparison with satellite-based estimates, *Deep Sea Research Part II*, *49*, 1623 – 1644, doi:10.1016/S0967-0645(02)00004-8.

Schneider, B., L. Bopp, M. Gehlen, J. Segschneider, T. L. Frölicher, P. Cadule, P. Friedlingstein, S. C. Doney, M. J. Behrenfeld, and F. Joos (2008), Climate-induced interannual variability of marine primary and export production in three global coupled climate carbon cycle models, *Biogeosciences*, *5*, 597–614, doi:10.5194/bg-5-597-2008.

Szeto, M., P. J. Werdell, T. S. Moore, and J. W. Campbell (2011), Are the world's oceans optically different?, *Journal of Geophysical Research*, *116, C00H04*, doi:10.1029/2011JC007230.

Takahashi, T., S. C. Sutherland, R. Wanninkhof, C. Sweeney, R. A. Feely, D. W. Chipman, B. Hales, G. Friederich, F. Chavez, C. Sabine, A. Watson, D. C. E. Bakker, U. Schuster, N. Metzl, H. Yoshikawa-Inoue, M. Ishii, T. Midorikawa, Y. Nojiri, A. Körtzinger, T. Steinhoff, M. Hoppema, J. Olafsson, T. S. Arnarson, B. Tilbrook, T. Johannessen, A. Olsen, R. Bellerby, C. S. Wong, B. Delille, N. R. Bates, and H. J. W. De Baar (2009), Climatological mean and decadal change in surface ocean pCO_2, and net sea-air CO_2 flux over the global oceans, *Deep Sea Research Part II: Topical Studies in Oceanography*, *56*, 554–577, doi:10.1016/j.dsr2.2008.12.009.

Wagener, T., C. Guieu, R. Losno, S. Bonnet, and N. Mahowald (2008), Revisiting atmospheric dust export to the Southern Hemisphere ocean: Biogeochemical implications, *Global Biogeochemical Cycles*, *22, GB2006*, doi:10.1029/2007GB002984.

Westberry, T., M. J. Behrenfeld, D. A. Siegel, and E. Boss (2008), Carbon-based primary productivity modeling with vertically resolved photoacclimation, *Global Biogeochemical Cycles*, *22, GB2024*, doi:10.1029/2007GB003078.

Whitworth, T. (1983), Monitoring the transport of the Antarctic Circumpolar Current at Drake Passage, *Journal of Physical Oceanography*, *13*, 2045–2057.

Whitworth, T., and R. G. Peterson (1985), Volume transport of the Antarctic Circumpolar Current from bottom pressure measurements, *Journal of Physical Oceanography*, *15*, 810–816.